Published in final edited form as:

Osteoarthritis Cartilage. 2023 January ; 31(1): 126–133. doi:10.1016/j.joca.2022.09.008.

In vivo Intervertebral Disc Mechanical Deformation Following a Treadmill Walking "Stress Test" is Inversely Related to T1rho Relaxation Time

James A. Coppock, MS[1,2], **Nicole E. Zimmer**[1,2], **Zoë A. Englander, PhD**[1,2], **Stephanie T. Danyluk, MS**[2], **Andrzej S. Kosinski, PhD**[3,4], **Charles E. Spritzer, MD**[5], **Adam P. Goode, DPT, PhD**[2,4,6], **Louis E. DeFrate, ScD**[1,2,7]

[1]Department of Biomedical Engineering, Duke University, Durham, North Carolina, USA

[2]Department of Orthopedic Surgery, Duke University School of Medicine, Durham, North Carolina, USA

[3]Department of Biostatistics & Bioinformatics, Duke University, Durham, North Carolina, USA

[4]Duke Clinical Research Institute, Duke University School of Medicine, Durham, North Carolina, USA

[5]Department of Radiology, Duke University School of Medicine, Durham, North Carolina, USA

[6]Department of Population Health Sciences, Duke University, Durham, North Carolina, USA

[7]Department of Mechanical Engineering and Materials Science, Duke University, Durham, North Carolina, USA

Abstract

Objective: To assess the *in vivo* relationship between the mechanical response of intervertebral discs (IVDs) to dynamic activity and IVD biochemical composition assessed via T1rho relaxation imaging.

Design: Eighteen asymptomatic participants with no history of low back pain (LBP), injury, or surgery underwent magnetic resonance (MR) imaging of their lumbar spine prior to and

Corresponding Author: Louis E. DeFrate, Sc.D., Room 379 Medical Sciences Research Bldg, Box 3093, Duke University Medical Center, Durham, NC 27710, 919-681-9959 (voice), lou.defrate@duke.edu.

AUTHOR CONTRIBUTIONS

JAC: Conceptualization, Methodology, Software, Validation, Formal analysis, Investigation, Data curation, Writing – Original draft preparation, Writing – Reviewing and Editing; **NEZ:** Validation, Data curation, Writing – Reviewing and Editing; **ZAE:** Conceptualization, Methodology, Writing – Reviewing and Editing; **STD:** Project administration, Investigation, Writing - Review & Editing; **ASK:** Methodology, Formal analysis, Writing - Review & Editing; **CES:** Methodology, Investigation, Writing - Review & Editing; **APG:** Conceptualization, Methodology, Resources, Supervision, Project administration, Funding acquisition, Methodology, Investigation, Writing - Review & Editing; **LED:** Conceptualization, Methodology, Resources, Supervision, Project administration, Funding acquisition, Investigation, Writing - Review & Editing.

CONFLICTS OF INTEREST

The authors declare that they have no known competing financial interests or personal relationships that could have appeared to influence the work reported in this paper.

immediately following a treadmill walking “stress test.” Anatomic (SPACE, FLASH) MR images were obtained pre- and post-exercise and utilized to measure IVD mechanical deformation. Quantitative (T1rho) imaging was performed pre-exercise to reflect IVD composition. Pre-exercise anatomic images were also utilized to assess IVD degenerative status based on the modified Pfirrmann scale. To quantify mechanical response, 3D surface models of the L1-L2–L5-S1 IVDs were created from manual segmentations of pre- and post-exercise anatomic images and utilized to assess changes in IVD height. IVD strain (%) was defined as change in IVD height normalized to pre-activity height. Linear mixed models were used to assess the relationships between IVD mechanical deformation (strain), composition (T1rho relaxation time), and degenerative status (Pfirrmann grade).

Results: Increased compressive IVD strain was associated with lower T1rho relaxation times in the nucleus pulposus (NP) of the disc ($\beta_{T1rho} = 5.07$, *CI*: [1.52, 7.77], $R^2_{marg} = 0.52$, $p = 0.005$). Thus, an inverse relationship between IVD strain and NP T1rho relaxation time was observed.

Conclusion: The *in vivo* mechanical response of the IVD to the “stress test” was sensitive to differences in NP composition. The results of this study suggest that quantification of *in vivo* IVD mechanical function and composition may provide insight into IVD health.

Keywords

intervertebral disc strain; low back pain; quantitative magnetic resonance imaging; in vivo biomechanics; precision medicine; diagnostic image analysis

INTRODUCTION

Low back pain (LBP) is a leading cause of disability worldwide[1–3]. Current diagnostic protocols commonly employ static (i.e., single time-point) imaging in order to identify potential sources of pain through evaluation of spinal anatomy[4–6]. However, the underlying sources of pain may be unclear on these static images[2, 7]. While the causes of LBP are multifactorial[1, 2, 8], intervertebral disc (IVD) degeneration has been identified as a risk factor for LBP development[4, 9, 10].

IVD degeneration is often characterized by changes in tissue biochemical composition, particularly loss of water and proteoglycans in the nucleus pulposus (NP)[11]. *Ex vivo* analyses have noted that degenerative changes are associated with decreased extracellular matrix production, increased catabolic enzyme production and increased inflammatory cytokine concentrations[12, 13]. Further *ex vivo* evidence suggests that tissue mechanics are altered in degenerated IVDs[11, 14, 15]. However, the effects of IVD tissue composition on *in vivo* mechanical function remain unclear.

To address these questions, our lab has developed and validated methods of non-invasively evaluating the mechanical response of IVDs to physiologic loading *in vivo*[16–18]. Specifically, we developed a technique to measure IVD deformation, defined as percent change in IVD height, resulting from an exercise “stress test.” In this technique, pre- and post-exercise magnetic resonance (MR) images are utilized to create 3D surface models of the IVDs[16], which are used to assess changes in IVD height following exercise. Additionally, T1rho relaxation imaging, a quantitative MR imaging technique, has garnered

interest as a potential method to identify early signs of IVD degeneration[10, 19–21] due to its sensitivity to proteoglycan and water concentrations in the IVD[10, 19–23]. Together, these techniques have the potential to measure both the mechanical function and composition of the IVD *in vivo* [19, 20, 22, 24].

Therefore, the purpose of this study was to explore the relationship between IVD deformations resulting from dynamic loading administered via a treadmill walking "stress test" and IVD biochemical composition, measured via T1rho relaxation times. Based on previous studies which have observed that IVD mechanics may be altered by altered IVD composition[19–24], we hypothesized that there would be an inverse relationship between IVD compressive deformations and T1rho relaxation times, such that increased compressive IVD deformations would be associated with lower T1rho relaxation times.

METHODS

Exploratory Data Analysis, Power Analysis and Sample Size Estimation

We used linear mixed-effects models to determine the relationship between BMI, T1rho relaxation times, and IVD deformations across different lumbar IVD levels. Specifically, measurements were repeated within subjects at five lumbar IVD levels (i.e., L1-L2 – L5-S1). To determine which covariance structure would be most suitable for this linear mixed-effects analysis, an exploratory analysis examining the pairwise correlation between within-subjects IVD deformations at successive lumbar levels (i.e., L1-L2 – L5-S1) was conducted. Results of this analysis suggested that IVD deformations were not compound symmetric (i.e., non-homogenous) as a function of IVD level. Rather, the correlation of measures made within-subjects decayed with increasing spatial separation between discs. Because of this, all linear mixed-effects models developed in this study utilized a first-order autoregressive correlation structure within subjects for parameter estimation, in favor of the compound symmetric structure.

Using pilot data from a previously published study[16], a power analysis was conducted to estimate the sample size of IVDs required to assess the effect of T1rho relaxation time on IVD deformations while accounting for BMI and IVD level. To do so, a multiple linear regression analysis was utilized[25, 26]. Accordingly, two linear mixed-effects models representing the reduced (MA: including BMI, and IVD level as predictors of IVD deformations) and full model (M_{AB}: including BMI, IVD level and T1rho relaxation times as predictors of IVD deformations) were fitted. In these analyses, BMI, and IVD level were included as potential confounding predictors of IVD deformations, because they represent physical attributes which may affect the magnitude of IVD loading during activities of daily living[16, 27–29].

Following model parameter estimation based on pilot data, the marginal coefficients of determination from the two models (i.e., M_A, M_{AB}) were then extracted, yielding $R^2_{M_A} = 0.42$ and $R^2_{M_{AB}} = 0.51$, respectively[26]. Effect size was then determined using Cohen's f^2, whereby $f^2 = \left(R^2_{M_{AB}} - R^2_{M_A}\right)/\left(1 - R^2_{M_A}\right) = 0.19$. The pwr.f2.test function from R's PWR (version 1.3–0) library was then used to estimate the denominator degrees of freedom (DF) from an

F-test with 1 DF in the numerator (one parameter due to T1rho added to the null model), considering α (0.05) and power (0.90). Results from this analysis indicated that a sample size of 76 IVDs would be sufficient to determine whether the inclusion of T1rho relaxation times enhanced the predictive power of estimating IVD deformations over the reduced model, if Cohen's f^2 is indeed of the specified magnitude. Therefore, IVD levels L1-L2 – L5-S1 across 18 subjects (5 IVDs * 18 subjects = 90 IVDs) were analyzed in this study.

Subject Recruitment and MR Imaging Parameters

Eighteen asymptomatic subjects participated in this institutional review board (IRB) approved study (Table 1). Deformation data from eight (L3-L4 – L5-S1) of the 18 subjects (25.8%; 23/89 IVDs) were part of a previously published pilot study[16]. Here, MR imaging was used to assess uniaxial IVD deformations by assessing changes in IVD height between pre- and post-exercise images and composition via T1rho relaxation times *in vivo*. MR images were obtained using a 3.0T scanner (Tim Trio, Siemens Medical Solutions) and 12-channel spine matrix coil. The MR sequence parameters utilized in this study are outlined in Table 2.

Imaging and Exercise Stress Test Protocol

To minimize the effects of diurnal changes in disc height,[30] subjects rested in a supine position for 45 minutes prior to the pre-exercise imaging. Following the rest period, subjects were then transported supine via a stretcher to the scanner for the pre-exercise MR scan. During the pre-exercise scan, a quantitative T1rho MR sequence (n = 18 subjects) was performed on all subjects. Additionally, anatomical MR sequences were acquired to evaluate and define IVD geometry. Specifically, a Sampling Perfection with Application optimized Contrasts using different flip angle Evolution (SPACE) scan was performed in all 18 subjects. Meanwhile, a Fast Low-Angle Shot (FLASH) sequence was obtained in 2 initial subjects. All subjects then completed an exercise "stress test", which involved walking on a treadmill for 30 min at a constant speed. The walking speed for each participant was normalized according to the length of their dominate leg using a Froude number (Fr) equal to 0.25[31, 32], resulting in an average walking speed of 1.5 m/s (range: 1.37–1.66 m/s, 3.1–3.7 mph). Limb length was defined as the vertical distance from the ground to the greater trochanter of the femur. Following the cessation of the stress test, subjects walked themselves to the MR scanner where post-exercise anatomic images were acquired using either the SPACE (n = 16 subjects) or the FLASH (n = 2 subjects) sequence.

Assessment of Pfirrmann Grade and Degeneration Status

IVD degeneration was assessed by a musculoskeletal radiologist using a pre-exercise mid-sagittal SPACE image for each subject according to the guidelines set forth by the 8-point modified Pfirrmann grading scale[33]. IVDs were then classified as either non-degenerative (Pfirrmann grades I-II) or degenerative (Pfirrmann grades III-VIII)[33]. Distribution of Pfirrmann grades by IVD level is detailed in Table 3.

IVD Deformation Analysis

IVD deformations were assessed via segmentation of MR images as described previously[16]. Briefly, a single investigator manually segmented the outer surfaces of the L1-L2 – L5-S1 IVDs in both the pre- and post-exercise anatomic scans. A musculoskeletal radiologist with more than 30 years of experience trained the investigator and reviewed all segmentations. During segmentation, the investigator was blinded to subject descriptive characteristics and demographics, including sex, BMI, NP T1rho relaxation times and degeneration status (Pfirrmann grade). These segmentations were then used to generate 3D surface models of the IVDs using solid modeling software (Rhinoceros 3D 4.0, Robert McNeel and Associates, Seattle, WA) and Geomagic Wrap 2021 (3D Systems, Cary, NC)[16] (Figure 1 A–D). IVD height was calculated by isolating the superior and inferior surfaces of the IVD and subsequently estimated by calculating the mean distance between the two surfaces. After evaluating both pre- and post-exercise models, IVD deformation (%) was calculated and defined as the percent change in IVD height from pre- to post-exercise scans[16]. Using these methods, IVD height calculations have been shown to be repeatable to within 1% across repeated segmentations[16]. Additionally, prior work in our lab found comparable repeatability in disc heights between different days[17].

IVD Composition Analysis

Average T1rho relaxation times within the NP of each IVD were obtained to reflect IVD tissue composition. This analysis of IVD composition was performed using custom software developed in MATLAB (R2021b) (MathWorks, Inc., Natick, MA). Specifically, IVD surface models were superimposed onto the T1rho image volumes in order to isolate the NP region of the disc. The NP region was isolated by extracting voxels within 50% of the radial distance from the IVD centroid to the boundary of the IVD surface model[16, 17].

To register IVD surface models to the T1rho images, first the T1rho images were cropped (Figure 1E) to isolate a single IVD of interest. Using an IVD-specific signal intensity threshold, a binary volumetric mask of the IVD was then created in order to approximate the centroid of the IVD in the T1rho image volume. Then, the surface model derived from the anatomic MR images was aligned with the volumetric T1rho mask at its centroid. The surface model was subsequently rigidly registered to the edges of the volumetric mask using an iterative closest point algorithm (Figure 1F). To refine the initial position of the surface model in the T1rho image volume, a custom graphical user interface (GUI) allowed the user to adjust the position of the IVD using six degrees-of-freedom rigid transformations. To assess model alignment in the T1rho image volume, the GUI visualizes both the 3D surface model (Figure 1F) and the segmentation masks (Figure 1G) created by the 3D position of the IVD model in the volume. The voxels contained within the surface model were then extracted for T1rho relaxation time analysis.

Once the position of the surface model in the T1rho image volume was determined, the T1rho relaxation time for each voxel (Figure 1H) contained within the surface model was calculated by fitting a mono-exponential decay function ($S(TSL) = S_0 \exp(-TSL/T1rho)$) to the signal intensities at each spin-lock time (TSL). In this equation, signal intensity at each TSL is denoted by $S(TSL)$, while S_0 is the maximum signal intensity, and $T1rho$ is the

relaxation time[32]. The NP region of the disc was then isolated from the whole-IVD model by extracting those voxels located within 50% of the radial distance from the IVD model's centroid[17, 18]. The average T1rho relaxation time within the NP region was then calculated for each subject and used in subsequent analyses.

Statistical Analyses

Routine descriptive characteristics (i.e., age, height, weight, body mass index (BMI)) were used to summarize (mean ± SD) subject demographics (Table 1). For all but one subject, measurements were obtained from the L1-L2 – L5-S1 IVDs. One L5-S1 IVD was excluded from analysis due to difficulties visualizing the IVD in the anatomic MR scan. Thus, IVD deformation and NP T1rho relaxation time measurements were obtained from 89 IVDs across the 18 subjects. All statistical models were developed in R statistical package version 4.1.2. (R Core Team, 2021) using the NLME package (3.1–153).

Kolmogorov-Smirnov tests suggested that T1rho relaxation data were non-normally distributed. Thus, prior to all analyses, a natural log transformation was applied to the NP T1rho relaxation time. In the first of two primary analyses, a linear mixed-effects model was developed to assess if NP T1rho relaxation times differed between degeneration groups (i.e., non-degenerative: Pfirrmann grades I-II; degenerative: Pfirrmann grades III-VIII). In this model, NP T1rho relaxation time was treated as the outcome measure, while degeneration status was treated as a fixed effect, and subject was treated as a random effect to account for correlation among measures within subjects.

We then assessed the effect of NP T1rho relaxation times on IVD deformation using a second linear mixed-effects model, whereby IVD deformation was the outcome measure. In this model, the relationship between IVD deformation and NP T1rho relaxation times was assessed while controlling for confounding factors: IVD level (categorical) and BMI (continuous). These factors were included as fixed main effects, as they may affect loading magnitude or resultant measured IVD deformation[16, 27, 28]. Prior work has demonstrated that T1rho relaxation times and Pfirrmann grades are collinear[10, 20]. Thus, degeneration status was not included in this model.

Furthermore, for both models, a sensitivity analysis was performed to assess the stability of the parameter estimations to the imaging sequences used for manual segmentation. Accordingly, data from the two subjects whose manual segmentations were performed using FLASH images was omitted and the linear mixed-effects models re-fitted; results from this analysis did not appreciably affect model parameters (< |10|% change in all β values) or model interpretation. As such, all subject data was retained in our final models. P-values less than established *a priori* $\alpha = 0.05$ indicate statistical significance. Kolmogorov-Smirnov tests were utilized to assess normality of the model residuals.

RESULTS

NP T1rho Relaxation Times and IVD Degeneration Status

NP T1rho relaxation times were lower ($\beta_{Degen} = -0.23$, *CI*: [−0.37, −0.23], $p < 0.0001$) in degenerative IVDs (Pfirrmann grades III-VIII) as compared to non-degenerative IVDs (Pfirrmann grades I-II).

IVD Deformation and NP T1rho Relaxation Times

The mean deformation across all IVDs was −6.5 ± 4.0%. Importantly, this study revealed that increased compressive IVD deformation ($\beta_{T1rho} = 5.07$, *CI*: [1.63, 8.52], $R^2_{marg} = 0.52$, $p = 0.005$) was associated with lower NP T1rho relaxation times while controlling for BMI and IVD level (Figure 2). Thus, an inverse relationship between IVD deformation and NP T1rho relaxation time was observed.

Post-Hoc Model Diagnostic Analyses

Kolmogorov-Smirnov tests did not detect that model residuals were non-normally distributed for the relationship between IVD composition and mechanical function (p = 0.987) or for the relationship between NP T1rho relaxation time and degeneration status (p = 0.858).

DISCUSSION

In this study, we investigated the relationship between *in vivo* IVD deformations resulting from a treadmill walking “stress test” and IVD composition as reflected by NP T1rho relaxation times. While controlling for IVD level and BMI, we observed an inverse relationship between compressive IVD deformations and NP T1rho relaxation times. Thus, the results of this study indicate that the *in vivo* mechanical response of the IVD is sensitive to NP composition as assessed via T1rho relaxation imaging.

Our results indicate that degenerated discs (Pfirrmann grades III-VIII) have NP T1rho relaxation times that are approximately 20ms lower than the group of non-degenerative IVDs. The results of these analyses are consistent with prior work[10, 19, 23, 24, 34], which has observed that T1rho relaxation times decrease as degeneration progresses, and is attributable to changes in IVD composition. As previously noted, degeneration status was not included in our primary model because Pfirrmann grades and NP T1rho relaxation times are collinear[10, 20], which is consistent with the findings of our model relating T1rho relaxation times to degeneration status.

We observed a mean compressive deformation of 6.5% across all IVDs. Interestingly, despite differences in both loading protocols (e.g., treadmill walking vs. loading apparatus) and measurement techniques, Chan and Neu (2014) observed similar mean IVD deformations (nominal strain = −5.9%)[35]. Importantly, in our study, the fitted parameter estimates suggested that a 1% decrease in measured IVD compression would be expected for every 20ms increase in mean NP T1rho relaxation time. Thus, the results of this study agree with prior *ex vivo* works which have found that degenerated IVDs[15, 27, 36, 37] and those with experimentally-manipulated NP composition[11, 19, 22–24, 37–40] demonstrate

altered mechanics. Specifically, prior studies have observed that changes in proteoglycan and water concentrations are related to altered IVD tissue stiffness[37, 38], stress and strain distributions[27, 40], fluid recovery[19, 36, 39] and failure mechanisms (e.g., herniation, delamination, fissure)[11, 40]. These changes are hypothesized to arise due to the loss of hydrophilic proteoglycans, which are largely responsible for generating osmotic and swelling pressures in the IVD tissues[38, 39, 41]. In the healthy IVD, these pressure gradients allow the NP to exert hydrostatic pressure onto the lamellae of the adjacent annulus fibrosus (AF) when the IVD is loaded[11, 15]. This hydrostatic pressure creates circumferential tension within the AF, augmenting the structural stiffness of the IVD and improving its resistance to compressive forces[11, 15]. Diminished pressurization of the NP has been shown to place an increased load-bearing burden on the AF[11, 40]. Thus, in the present study, the increasing compressive deformations observed in IVDs with lower T1rho relaxation times, may be related to these altered load-bearing mechanisms observed in prior *ex vivo* studies[13, 15, 19, 27, 36–39].

When considering the development of LBP, the observation that distinct stress distributions and failure mechanisms occur in degenerated IVDs as compared to healthy IVDs is of particular interest. To this point, the presence of nervous fibers in the inner AF and NP has been observed in both human and animal models of IVD degeneration and LBP[42–45], suggesting that IVD degeneration may lead to innervation of deeper tissue structures beyond the outermost layers of the IVD[42]. Furthermore, it was recently observed that innervation of degenerated IVDs may specifically occur in mechanically disrupted tissues (e.g., annular fissures)[43]. Additionally, prior studies have demonstrated that proteoglycans in tissue culture inhibit nervous fiber growth[43, 46, 47]. Together, these findings suggest that structural tissue disruptions and loss of proteoglycans in IVDs may potentiate degenerative processes which provide a mechanism for the onset of discogenic LBP[43]. In light of these findings, future *in vivo* analyses which evaluate the longitudinal relationship between IVD composition and mechanical function in individuals who develop acute and chronic LBP will be integral to understanding how these factors may change and play a role in the development of LBP.

While every effort was made to minimize the time elapsed between the end of the walking exercise and the start of post-exercise imaging, it is likely that some recovery occurred prior to and during the post-exercise MRI[48], resulting in underestimates in our measurements of compressive deformation. Despite this potential for underestimating deformations immediately after exercise, we were still able to detect relationships between IVD composition and deformation in this study. In comparison to similar *ex vivo* analyses[15, 19, 27, 36, 40], studies examining *in vivo* tissue mechanics tend to have relatively coarse sampling resolutions. However, future work which leverages recent improvements to both spatial[40, 49, 50] and temporal[49] resolutions in MR imaging may enable finer characterization of IVD mechanics *in vivo*.

Finally, in this study, the boundaries between the NP and AF were delineated by isolating the voxels within 0–50% of the radial distance from the centroid of the 3D surface model. While this technique does not consider subject-specific anatomical differences in NP geometry, the use of a pre-defined NP boundary is consistent with prior imaging studies[10, 17, 18, 20, 23, 34]. Nevertheless, exploration of alternative methods for identifying

anatomic boundaries within the IVD, therefore, may be useful as a way for validating or improving upon current methods. Despite this limitation, the NP T1rho relaxation times observed in this study were consistently higher than those in the surrounding regions. This finding is consistent with prior work quantifying the relationship between regional IVD anatomy and T1rho relaxation times[19, 23, 24, 41].

In conclusion, this study investigated how *in vivo* IVD mechanical function relates to IVD composition in a relatively young, asymptomatic sample of individuals. The results of this study indicate that the mechanical response of IVDs to dynamic in vivo loading are sensitive to the composition of the NP, as measured by T1rho relaxation times. Finally, the results of this study suggest that quantification of *in vivo* IVD mechanical function with respect to its composition may be a useful tool in understanding the development of IVD degeneration and discogenic LBP.

ACKNOWLEDGEMENTS

We would like to thank Jean Shaffer and Raven Boykin at the Duke Center for Advanced Magnetic Resonance Development for their continued help and support.

ROLE OF THE FUNDING SOURCE

This work was supported by NIH grants AR074800, AR065527, AR075399, and AR071440.

REFERENCES

1. Hoy D, Brooks P, Blyth F, Buchbinder R. The epidemiology of low back pain. Best Practice and Research: Clinical Rheumatology 2010; 24: 769–781. [PubMed: 21665125]
2. Maher C, Underwood M, Buchbinder R. Non-specific low back pain. Lancet 2017; 389: 736–747. [PubMed: 27745712]
3. Taylor JB, Goode AP, George SZ, Cook CE. Incidence and risk factors for first-time incident low back pain: A systematic review and meta-analysis. Spine Journal 2014; 14: 2299–2319.
4. Raastad J, Reiman M, Coeytaux R, Ledbetter L, Goode AP. The association between lumbar spine radiographic features and low back pain: A systematic review and meta-analysis. Seminars in Arthritis and Rheumatism 2015; 44: 571–585. [PubMed: 25684125]
5. Steffens D, Hancock MJ, Maher CG, Williams C, Jensen TS, Latimer J. Does magnetic resonance imaging predict future low back pain? A systematic review. European Journal of Pain 2014; 18: 755–765. [PubMed: 24276945]
6. Tonosu J, Oka H, Higashikawa A, Okazaki H, Tanaka S, Matsudaira K, et al. The associations between magnetic resonance imaging findings and low back pain: A 10-year longitudinal analysis. PLoS One 2017; 12: e0188057. [PubMed: 29141001]
7. Koes BW, Van Tulder MW, Thomas S. Diagnosis and treatment of low back pain. BMJ 2006; 332: 1430–1434. [PubMed: 16777886]
8. Fujii K, Yamazaki M, Kang JD, Risbud MV, Cho SK, Qureshi SA, et al. Discogenic Back Pain: Literature Review of Definition, Diagnosis, and Treatment. JBMR Plus 2019; 3: e10180. [PubMed: 31131347]
9. Shiri R, Karppinen J, Leino-Arjas P, Solovieva S, Viikari-Juntura E. The association between obesity and low back pain: A meta-analysis. American Journal of Epidemiology 2010; 171: 135–154. [PubMed: 20007994]
10. Borthakur A, Maurer PM, Fenty M, Wang C, Berger R, Yoder J, et al. T1ρ MRI and Discography Pressure as Novel Biomarkers for Disc Degeneration and Low Back Pain. Spine 2011; 36: 2190–2196. [PubMed: 21358489]

11. Adams MA, Roughley PJ. What is intervertebral disc degeneration, and what causes it? Spine 2006; 31: 2151–2161. [PubMed: 16915105]
12. Kepler CK, Ponnappan RK, Tannoury CA, Risbud MV, Anderson DG. The molecular basis of intervertebral disc degeneration. The Spine Journal 2013; 13: 318–330. [PubMed: 23537454]
13. Vergroesen P-PA, Kingma I, Emanuel KS, Hoogendoorn RJW, Welting TJ, Van Royen BJ, et al. Mechanics and biology in intervertebral disc degeneration: a vicious circle. Osteoarthritis and Cartilage 2015; 23: 1057–1070. [PubMed: 25827971]
14. Adams MA. Intervertebral Disc Tissues. In: Mechanical Properties of Aging Soft Tissues, Derby B, Akhtar R Eds. New York: Springer 2015:7–35.
15. Newell N, Little JP, Christou A, Adams MA, Adam CJ, Masouros SD. Biomechanics of the human intervertebral disc: A review of testing techniques and results. Journal of Mechanical Behavior of Biomedical Materials 2017; 69: 420–434.
16. Coppock JA, Danyluk ST, Englander ZA, Spritzer CE, Goode AP, DeFrate LE. Increasing BMI increases lumbar intervertebral disc deformation following a treadmill walking stress test. Journal of Biomechanics 2021; 121: 110392. [PubMed: 33819699]
17. Martin JT, Oldweiler AB, Spritzer CE, Soher BJ, Erickson MM, Goode AP, et al. A magnetic resonance imaging framework for quantifying intervertebral disc deformation in vivo: Reliability and application to diurnal variations in lumbar disc shape. Journal of Biomechanics 2018; 71: 291–295. [PubMed: 29456171]
18. Martin JT, Oldweiler AB, Kosinski AS, Spritzer CE, Soher BJ, Erickson MM, et al. Lumbar intervertebral disc diurnal deformations and T2 and T1rho relaxation times vary by spinal level and disc region. European Spine Journal 2022.
19. Paul CPL, Smit TH, de Graaf M, Holewijn RM, Bisschop A, van de Ven PM, et al. Quantitative MRI in early intervertebral disc degeneration: T1rho correlates better than T2 and ADC with biomechanics, histology and matrix content. PLoS One 2018; 31: e0191442.
20. Zobel BB, Vadalà G, Vescovo RD, Battisti S, Martina FM, Stellato L, et al. T1 ρ Magnetic resonance imaging quantification of early lumbar intervertebral disc degeneration in healthy young adults. Spine 2012; 37: 1221–1230.
21. Wáng YX, Zhang Q, Li X, Chen W, Ahuja A, Yuan J. T1ρ magnetic resonance: basic physics principles and applications in knee and intervertebral disc imaging. Quant Imaging Med Surg 2015; 5: 858–885. [PubMed: 26807369]
22. Antoniou J, Mwale F, Demers C, Gilles B, Tapas G, Aegi M, et al. Quantitative magnetic resonance imaging of enzymatically induced degradation of the nucleus pulposus of intervertebral discs. Spine 2006; 31: 1547–1554. [PubMed: 16778686]
23. Johannessen W, Auerbach J, Wheaton A, Kurji A, Borthakur A, Reddy R, et al. Assessment of human disc degeneration and proteoglycan content using T1ρ-weighted magnetic resonance imaging. Spine (Phila Pa 1976) 2006; 31: 1253–1257. [PubMed: 16688040]
24. Mwale F, Demers CN, Michalek AJ, Beaudoin G, Goswami T, Beckman L, et al. Evaluation of quantitative magnetic resonance imaging, biochemical and mechanical properties of trypsin-treated intervertebral discs under physiological compression loading. Journal of Magnetic Resonance Imaging 2008; 27: 563–573. [PubMed: 18219615]
25. Cohen J Statistical Power Analysis for the Behavioral Sciences 2013.
26. Selya AS, Rose JS, Dierker LC, Hedeker D, Mermelstein RJ. A practical guide to calculating Cohen's f(2), a measure of local effect size, from PROC MIXED. Frontiers in Psychology 2012; 3.
27. O'Connell GD, Vresilovic EJ, Elliott DM. Human intervertebral disc internal strain in compression: The effect of disc region, loading position, and degeneration. Journal of Orthopaedic Research 2011; 29: 547–555. [PubMed: 21337394]
28. Ghezelbash F, Shirazi-Adl A, Plamondon A, Arjmand N, Parnianpour M. Obesity and Obesity Shape Markedly Influence Spine Biomechanics: A Subject-Specific Risk Assessment Model. Annals of Biomedical Engineering 2017; 45: 2373–2382. [PubMed: 28608245]
29. Han KS, Rohlmann A, Zander T, Taylor WR. Lumbar spinal loads vary with body height and weight. Med Eng Phys 2013; 35: 969–977. [PubMed: 23040051]
30. Adams MA, Doland P, Hutton WC, Porter RW. Diurnal changes in spinal mechanics and their clinical significance. Journal of Bone and Joint Surgery Br 1990; 72: 266–270.

31. Paranjape CS, Cutcliffe HC, Grambow SC, Utturkar GM, Collins AT, Garrett WE, et al. A New Stress Test for Knee Joint Cartilage. Scientific Reports 2019; 9.
32. Collins AT, Kulvaranon ML, Cutcliffe HC, Utturkar GM, Smith WAR, Spritzer CE, et al. Obesity alters the in vivo mechanical response and biochemical properties of cartilage as measured by MRI. Arthritis Research & Therapy 2018; 20.
33. Griffith JF, Wang YX, Antonio GE, Choi KC, Yu A, Ahuja AT, et al. Modified Pfirrmann grading system for lumbar intervertebral disc degeneration. Spine 2007; 32: E708–712. [PubMed: 18007231]
34. Yoon MA, Hong SJ, Kang CH, Ahn KS, Kim BH, T1rho and T2 mapping of lumbar intervertebral disc: Correlation with degeneration and morphologic changes in different disc regions. Magnetic Resonance Imaging 2016; 37: 932–939.
35. Chan DD, Neu CP. Intervertebral disc internal deformation measured by displacements under applied loading with MRI at 3T. Magnetic Resonance in Medicine 2014; 71: 1231–1237. [PubMed: 23650022]
36. O'Connell GD, Jacobs NT, Sen S, Vresilovic EJ, Elliott DM. Axial creep loading and unloaded recovery of the human intervertebral disc and the effect of degeneration. Journal of Mechanical Behavior of Biomedical Materials 2011; 4: 933–942.
37. Vergroesen PPA, Emanuel KS, Peeters M, Kingma I, Smit TH. Are axial intervertebral disc biomechanics determined by osmosis? Journal of Biomechanics 2018; 70: 4–9. [PubMed: 28579261]
38. Bezci SE, Nandy A, O'connell GD. Effect of Hydration on Healthy Intervertebral Disk Mechanical Stiffness. Journal of Biomechanical Engineering 2015; 137: 101007. [PubMed: 26300418]
39. Bezci SE, O'Connell GD, Osmotic Pressure Alters Time-dependent Recovery Behavior of the Intervertebral Disc. Spine (Philadelphia, Pa.: 1986) 2018; 43: E334–340.
40. Tavana S, Masouros SD, Baxan N, Freedman BA, Hansen UN, Newell N. The Effect of Degeneration on Internal Strains and the Mechanism of Failure in Human Intervertebral Discs Analyzed Using Digital Volume Correlation (DVC) and Ultra-High Field MRI. Frontiers in Bioengineering and Biotechnology 2021; 8: 610907. [PubMed: 33553116]
41. Iatridis JC, Maclean JJ, O'Brien M, Stokes IAF. Measurements of Proteoglycan and Water Content Distribution in Human Lumbar Intervertebral Discs. Spine 2007; 32: 1493–1497. [PubMed: 17572617]
42. Groh AMR, Fournier DE, Battié MC, Séguin CA. Innervation of the Human Intervertebral Disc: A Scoping Review. Pain Medicine 2021; 22: 1281–1304. [PubMed: 33595648]
43. Lama P, Maitre CLL, Harding IJ, Dolan P, Adams MA. Nerves and blood vessels in degenerated intervertebral discs are confined to physically disrupted tissue. Journal of Anatomy 2018; 233: 86–97. [PubMed: 29708266]
44. Lee S, Millecamps M, Foster DZ, Stone LS, Long-term histological analysis of innervation and macrophage infiltration in a mouse model of intervertebral disc injury–induced low back pain. Journal of Orthopaedic Research 2020; 38: 1238–1247. [PubMed: 31814143]
45. Lyu F-J, Cui H, Pan H, Cheung KM, Cao X, Iatridis JC, et al. Painful intervertebral disc degeneration and inflammation: from laboratory evidence to clinical interventions. Bone Research 2021; 9: 7. [PubMed: 33514693]
46. Johnson WEB, Caterson B, Eisenstein SM, Hynds DL, Snow DM, Roberts S. Human intervertebral disc aggrecan inhibits nerve growth in vitro. Arthritis & Rheumatism 2002; 46: 2658–2664. [PubMed: 12384924]
47. Lee JM, Song JY, Baek M, Jung HY, Kang H, Han IB, et al. Interleukin-1β induces angiogenesis and innervation in human intervertebral disc degeneration. Journal of Orthopaedic Research 2011; 29: 265–269. [PubMed: 20690185]
48. Cutcliffe HC, Davis KM, Spritzer CE, Defrate L. The Characteristic Recovery Time as a Novel, Noninvasive Metric for Assessing In Vivo Cartilage Mechanical Function. Annals of Biomedical Engineering 2020; 48: 2901–2910. [PubMed: 32666421]
49. Menon RG, Zibetti MVW, Pendola M, Regatte RR. Measurement of Three-Dimensional Internal Dynamic Strains in the Intervertebral Disc of the Lumbar Spine With Mechanical Loading

and Golden-Angle Radial Sparse Parallel-Magnetic Resonance Imaging. Journal of Magnetic Resonance Imaging 2021; 54: 486–496. [PubMed: 33713520]

50. Wilson RL, Bowen L, Kim W, Cai L, Schneider SE, Nauman EA, et al. In vivo intervertebral disc deformation: intratissue strain patterns within adjacent discs during flexion–extension. Scientific Reports 2021; 11: 729. [PubMed: 33436667]

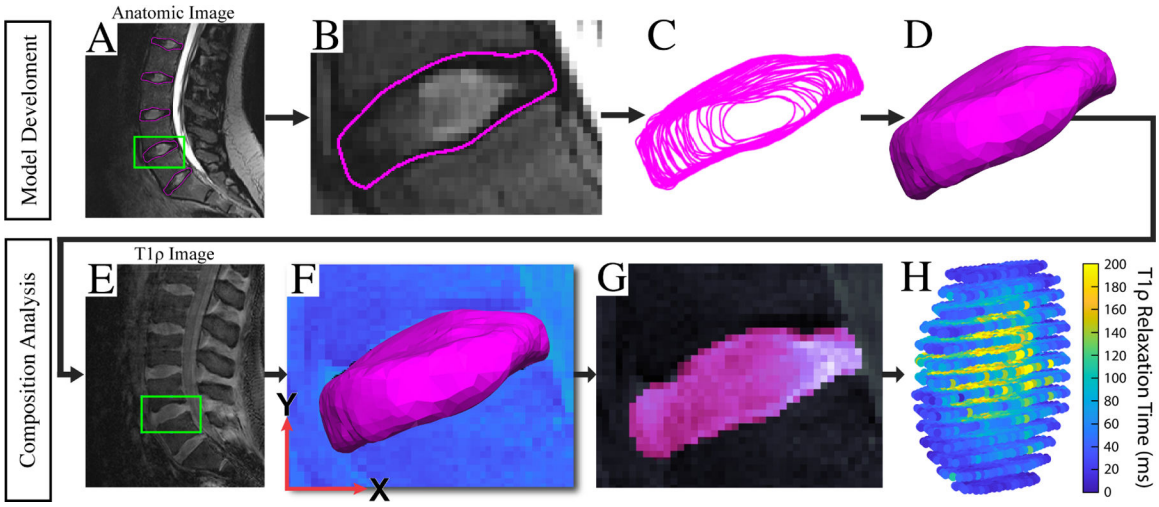

Figure 1: IVD Modeling and T1rho Relaxation Analysis Pipeline.

(**A/B/C)** IVD contours are manually segmented and transformed into wireframe models. **(D)** Solid modeling software is then used to develop 3D surface models of the IVDs. **(E)** T1rho image volumes were then cropped to isolate an IVD. Using an IVD-specific signal intensity threshold, a binary volumetric mask of the IVD was then created in order to approximate the centroid of the IVD in the T1rho image volume. **(F)** Then, the surface model derived from the anatomic MR images was aligned with the volumetric T1rho mask at its centroid and rigidly registered to the edges of the volumetric mask using an iterative closest point algorithm. **(G)** Ultimately, the voxels contained within the surface model were then utilized to generate segmentation masks of the IVD in the T1rho volume. To refine the initial position of the surface model in the T1rho image volume, a custom graphical user interface (GUI) allowed the user to adjust the position of the IVD using six degrees-of-freedom rigid transformations. (**F**) To assess model alignment in the T1rho image volume, the GUI visualizes both the 3D surface model and the segmentation masks (**G**) created by the 3D position of the IVD model in the volume. **(H)** Once the position of the surface model in the T1rho image volume was determined, the T1rho relaxation time for each voxel contained within the surface model was calculated. The NP region of the disc was then isolated from the whole-IVD model by extracting those voxels located within [0–50%] of the radial distance from the IVD surface model's centroid. The average T1rho relaxation time within the NP region was then calculated for each subject and used in future analyses.

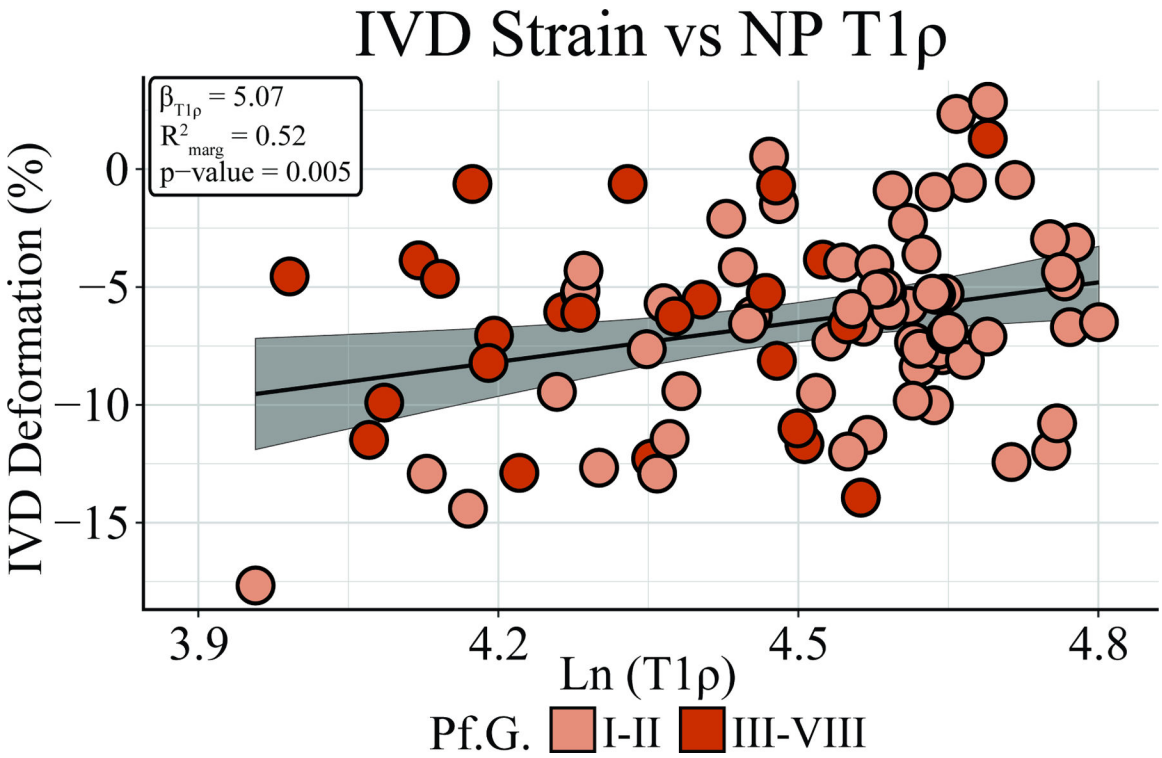

Figure 2: IVD Deformations are Inversely Associated with NP T1rho Relaxation Times.

Assessment of the relationship between IVD composition and mechanical function revealed that lower NP T1rho relaxation times were associated with increasing compressive IVD strain (β_{T1rho} = 5.07, CI: [1.52, 7.77], R^2_{marg} = 0.52, p = 0.005), while controlling for BMI and IVD level. Thus, an inverse relationship between NP T1rho relaxation time and IVD strain was observed. Degenerative status (determined by Pfirrmann grade) is denoted by light orange (non-degenerative) and dark orange (degenerative).

Table 1:

Subject Demographics

	Sex (n)	
Parameter	**Female (11)**	**Male (7)**
Age (years)	25.1 ± 3.1	31.4 ± 15.4
Height (m)	1.64 ± 0.06	1.84 ± 0.05
Weight (kg)	65.8 ± 13.4	92.0 ± 15.6
BMI (kg/m^2)	24.5 ± 4.9	27.1 ± 4.0

Table 2:

MR Sequence Parameters.

	Sequence		
Parameter	**FLASH**	**T2w SPACE**	**T1rho**
Purpose	3D Modeling	Pfirrmann grading/3D Modeling	Composition
Repetition Time (ms)	9.0	2500	4000
Echo Time (ms)	3.7	223	5.5
Spin Lock Times (ms)	-	-	2, 10, 20, 40, 60 (500 Hz)
Flip Angle (°)	14.88	100	15
Matrix Size (voxels)	224 × 256 × 64	320 × 320 × 80	256 × 256 × 26
Resolution (mm)	1.0 × 1.0 × 1.0	0.875 × 0.875 × 0.875	0.976 × 0.976 × 3.00

Table 3:

Pfirrmann Grade Count by level and degenerative status

	Pfirrmann Grade (I - VIII)							
	Non-degenerative (n = 63)		*Degenerative (n = 26)*					
IVD Level	**I**	**II**	**III**	**IV**	**V**	**VI**	**VII**	**VIII**
L1 – L2	-	15	3	-	-	-	-	-
L2 – L3	-	15	3	-	-	-	-	-
L3 – L4	-	15	2	-	1	-	-	-
L4 – L5	-	11	4	2	-	1	-	-
L5 – S1	-	7	6	1	-	2	-	1